Variational estimation of effective channel and ungauged anabranching river discharge from multi-satellite water heights of different spatial sparsity

Pierre-André Garambois, Kévin Larnier, Jerome Monnier, Pascal Finaud-Guyot, Jonas Verley, Amanda Samine Montazem, Stéphane Calmant

Variational inference of effective channel and ungauged anabranching river discharge from multi-satellite water heights of different spatial sparsity

P.-A. Garambois(1)(2)(3)*, K. Larnier(5)(2)(4)(6), J. Monnier (5)(6), P. Finaud-Guyot(7), J. Verley(5)(6), A.-S. Montazem(8)(9), S. Calmant (8)(9)

(1) Now at: Irstea, Aix Marseille Univ, RECOVER, Aix-en-Provence, France

(2) ICUBE, CNRS, Univ Strasbourg, France.

(3) INSA Strasbourg, Strasbourg, France

(4) CS corporation, Business Unit Espace, Toulouse, France

(5) Institut de Mathématiques de Toulouse (IMT), France

(6) INSA Toulouse, France

(7) Now at: HSM, Univ Montpellier, CNRS, IRD, Montpellier, France

(8) LEGOS, UMR 5566, CNES, CNRS, IRD, UPS,

(9) Université de Toulouse III Paul Sabatier, OMP, Toulouse, France

Abstract

Multi-satellite sensing of continental water surfaces (WS) represents an unprecedented and increasing potential for studying ungauged hydrological and hydraulic processes from their signatures, especially on complex flow zones such as anabranching rivers. However the estimation of discharge from WS observations only is a very challenging, ill-posed, inverse problem due to unknown bathymetry and friction in ungauged rivers, measurements nature, quality and spatio-temporal resolutions regarding the flow (model) scales. This paper proposes an effective 1D hydraulic modeling approach of sufficient complexity to describe anabranching river flows from sparse multisatellite observations using the HiVDI inverse method presented in [1] with an augmented control vector including a spatially distributed friction law $K(x,h)$ depending on the flow depth h. It is shown on $71km$ of the Xingu River (anabranching, Amazon basin) with altimetric water height timeseries that a fairly accurate upstream discharge hydrograph and effective patterns of channel bathymetry and friction can be infered simultaneously. The coherence between the sparse observation grid and the fine hydraulic model grid is ensured in the optimization process by imposing a piecewise linear bathymetry profile $b(x)$, which is consistent with the *hydraulic visibility* of WS signatures ([2, 3]). The discharge hydrograph Q(t) at observation times and effective bathymetry-friction ($b(x)$, $K(x,h)$) patterns are retrieved from 8 years of satellite altimetry (ENVISAT) at 6 virtual stations (VS) along flow. Next, the potential of the forthcoming SWOT data, dense in space, is highlighted by infering a discharge hydrograph and dense patterns of effective river bathymetry and friction; a physically consistent scaling of friction by reaches enables to consider more dense bathymetry controls. Finally a numerical analysis shows: (i) the importance of an unbiased prior information in the inference of a triplet $(Q, b(x), K(x,h))$ from WS observations; (ii) the clear signatures of river bottom slope break in low flows and width variations in high flows, through the analysis of the friction slope term, which is consistent with the findings of [3] from WS curvature analysis.

Keywords: Anabranching River, Ungauged River, 1D Hydraulic Model, Variational Assimilation, Satellite Altimetry, SWOT, Hydraulic Visibility

Corresponding author: pierre-andre.garambois@irstea.fr

1. Introduction

Fresh water is a crucial earth's resource and its journey from the clouds to the oceans passes through the hydrographic network. In order to characterize hydrological fluxes, an essential physical variable is river discharge (cf. Global Climate Observing system [4]) representing an integration of upstream hydrological processes. In complement of in situ sensors networks which are declining in some regions (e.g. [5]), increasingly accurate measurements of hydrological and hydraulic variables, and especially river surface variabilities are now enabled by myriads of satellites for earth observation and new generations of sensors (e.g. [6, 7, 8, 9]).

The forthcoming Surface Water and Ocean Topography (SWOT) wide swath altimetric mission (CNES-NASA, planned to be launched in 2021) will provide a quasi global river surfaces mapping with an unprecedented spatial and temporal resolution on Water Surface (WS) height, width and slope - decimetric accuracy on WS height averaged over 1 km^2, 1 to 4 revisits every 21 days cycle [10, 11, 12, 13, 14]. In addition to decades of nadir altimetry (e.g. [15, 16, 17, 18]) and imagery (e.g. [19]) on inland waters, SWOT will enable an unprecedented *hydraulic visibility,* as defined from hydraulic analysis in [2, 20, 3], of hydrological responses and hydraulic variabilities within river networks. Multi-satellite observations of water surfaces from the local to the hydrographic network scale indeed represent an unprecedented observability of hydrological responses through hydraulic processes signatures, especially on complex flow zones such as floodplains or anabranching rivers (see river morphology classification in [21]). This increased *hydraulic visibility* represents a great potential to learn hydrodynamic behaviors and infer hydrological fluxes.

The estimation of river discharge from water surface observations (elevations, top width) remains an open and difficult question, especially in case of unknown or poorly known river bathymetry, friction or lateral fluxes. Several open-channel inverse problems are studied in a relatively recent litterature in a satellite data context with more or less complex flow models and inverse methods (cf. [13] for a review). Few studies started to highlight the benefits of assimilating synthetic SWOT WS observations in simplified hydraulic models with sequential methods, for infering inflow discharge assuming known river friction and bathymetry [22, 23] or infering bathymetry assuming known friction [24, 25]. Next, low-complexity methods have been proposed for estimating river discharge in case of unknown bathymetry and friction based on the kinematic wave assumption [26, 27] or hydraulic geometries [28] or empirical flow models ([29], see also [30]). They are tested on 19 rivers with synthetic "SWOT-like" daily observations in [29] and their robustness and accuracy is found to fluctuate, the importance of good prior guesses

is highlighted.

The combined use of dynamic flow models and optimization methods enables to benefit from WS observations for solving hydraulic inverse problems as shown for flood hydrograph inference in [31] from WS width time series used to optimize a 1D hydraulic model or in [32, 33, 34] by variational assimilation of flow depth time series in a 2D hydraulic model. The variational data assimilation (VDA) approach (see e.g. [35] and references therein) is well suited to solve the present inverse problem (see [36, 37, 1] and references therein).

It consists in fitting the hydraulic model response to the observed WS elevations by optimizing the "input parameters" in a variational framework. However, altimetry measurements of WS are relatively sparse in time compared to local flow dynamics. This important aspect of the inverse problem is investigated in [36] with the introduction of *the identifiability maps*. The latter consist to represent in space-time the available information: WS observables, hydraulic waves and an estimation of the misfit with the local equilibrium. These "maps" enable to estimate if the sought upstream discharge information has been observed or not within the downstream river surface deformations; also they help to estimate inferable hydrograph frequencies [36] or inferable hydrograph time windows [1].

The inference of the hydraulic triplet (inflow discharge $Q(t)$, effective bathymetry $b(x)$ and friction coefficient K) from SWOT like WS observations is investigated in recent studies using 1D hydraulic and variational assimilation methods (e.g. [36, 38, 37, 1]). However the inference of the triplet from WS observations remains a very challenging inverse problem because of the correlated influence of temporal (discharge) and spatial (bathymetry-friction) controls on the simulated flow lines. This is especially true because of the bathymetry-friction "equifinality issue", see the discussions in [27, 1]. Those recently developed VDA methods enable to infer accurately the inflow discharge from water surface observables, considering unknown/uncertain channel bathymetry-friction, but from accurate prior information and synthetic WS observations. Note that a strong prior such as a known stage-discharge relationship (rating curve) downstream of a river domain as it is done in [37] can control part of the simulated flow lines (fluvial regime); as a consequence the VDA process may converge to the discharge hydrograph corresponding to the imposed (almost exact) rating curve. In the present study the downstream boundary condition (BC) is an unknown of the inverse problem.

A crucial point is the sensitivity of the triplet inference to the prior value from which the inference is started and it is studied in a SWOT observability context in [27, 39, 1, 40]. The sensitivity of the estimated discharge (in the triplet) to the prior is highlighted by recent estimates performed from AirSWOT airborne measurements on the Willamette River [40]. The temporal signal is well retrieved at observation times but using a biased prior hydrograph results in a biased hydrograph inference - see detailed investigations in [1]. In view to infer worldwide river discharges from the future SWOT observations, especially for ungauged cases, a hierarchical modeling strategy HiVDI (Hierarchical Variational Discharge Inversion) is proposed in [1]. The HiVDI approach includes low complexity flow relations (under the assumption of Low Froude and locally steady-state flows) which improves the robustness of the inferences

in particular if an (unbiaised) average value of Q is provided. (It may be provided by a database or a regional hydrological model). Note that if introducing an a-priori information such as a single depth measurement, it enables to reconstruct an effective low-flow bathymetry see [41, 27, 1].

All the studies mentioned above mostly address single channel natural rivers ($\sim$ 100km in length) without lateral inflows and using synthetic datasets (except in [40] with AirSWOT data). Moreover very few studies address the modeling of effective 1D channels from real satellite data (e.g. [2, 42]).

The present paper investigates the effective hydraulic modeling of anabranching river flows from real multi-sensor satellite observations of WS, the challenging inference of the hydraulic triplet ($Q(t)$, $b(x)$, $K(x,h)$) and its sensitivity to observation density in space. Anabranching rivers are characterized by complex hydraulic geometries relationships across flow regimes as shown in [43] through an analysis of a metric resolution 2D shallow water model of an anabranching portion of the Platte River, US. The key point here is to build up a sufficiently complex model to describe anabranching river flows and in coherence with the spatio-temporal scales of satellite altimetry measurements.

Based on the inverse method presented in [1, 36], an effective hydraulic modeling strategy is adapted for tackling anabranching river flows using: (i) effective 1D cross sections based on real multi-satellite data from low to high flows (ii) a spatially distributed friction law depending on modeled water depth h. The inference of distributed hydraulic parameters patterns is investigated on a $71km$ long reach of the Xingu River (Amazone basin) from real altimetric observations gained on a single ENVISAT track or from synthetic SWOT observations, low *identifiability index* (as introduced in [36] and detailed in section 4). The influence of the spatial density of WS observations on the identifiability of spatial controls patterns (in the unknown triplet) is studied. A piecewise linear bathymetry representation is introduced along with a friction power law with piecewise constant parameters to put in coherence the observations and the flow model grids. Their constraining effect on the inversions is studied with spatially (and temporally) sparse satellite observations. Furthermore, numerical investigations are performed to test the sensitivity of hydraulic inferences to prior hydraulic values and also assess the correlated influence of bathymetry and friction on the modeled flow lines (equifinality) across flow regimes.

This study is organized as follows. Section 2 presents the 1D Saint-Venant flow model and the effective modeling approach for anabranching rivers including: (i) a spatially distributed friction law depending on the modeled flow depth, (ii) the construction of an effective channel geometry from multi-satellite observations, (iii) an inverse method based on variational data assimilation. Section 3 focuses on the calibration of the effective model on 8 years of WS observations gained from ENVISAT altimeter on a single track along this anabranching river. Using this model as a reference, section 4 proposes detailed investigations of the hydraulic inferences from real ENVISAT or synthetic SWOT observations considering this anabranching river as ungauged. The discussion in section 5 presents a numerical sensitivity analysis to the hydraulic prior and some investigations on the bathymetry friction equifinality.

2. Modeling approach:

This section proposes an original 1D effective modeling approach of adequate complexity for modeling anabranching river flows across (fluvial) regimes and in coherence with satellite observations. The approach is built on an effective channel cross-section derived from multi-satellite measurements and a spatially distributed friction law depending on the flow depth.

2.1. The flow model

River flows are classically modeled using the 1D Saint-Venant shallow water equations involving an integration of the flow variables over the cross section (see e.g. [44, 45] for detailed assumptions). In (A, Q) variables, A the wetted-cross section $\left[\mathrm{m}^2\right]$, Q the discharge $\left[\mathrm{m}^3.\mathrm{s}^{-1}\right]$, the equations read as follows [44]:

$$\begin{cases} \partial_t(A) + \partial_x(Q) & = 0 \\ \partial_t Q + \partial_x\left(\frac{Q^2}{A}\right) & = -gA\,\partial_x Z - gAS_f \end{cases} \tag{1}$$

where g is the gravity magnitude $\left[\mathrm{m.s}^{-2}\right]$, Z is the WS elevation [m], $Z = (b+h)$ with b is the river bottom elevation [m] and h is the water depth [m]. The friction slope S_f is parameterized with the classical Manning-Strickler law such that $S_f = {}^{|Q|Q}/_{K^2A^2R_h^{4/3}}$ with K the Strickler friction coefficient $\left[\mathrm{m}^{1/3}.\mathrm{s}^{-1}\right]$, $R_h = {}^{A}/_{P_h}$ the hydraulic radius [m] , P_h the wetted perimeter. The discharge Q is related to the average cross-sectional velocity u $\left[\mathrm{m.s}^{-1}\right]$ such as $Q = uA$. A spatially distributed Strickler friction coefficient is defined as a power law in the water depth h:

$$K(x, h(x,t)) = \alpha(x) h(x,t)^{\beta(x)} \tag{2}$$

where α and β are two constants. Similar approaches based on hydraulic geometry or power law resistance equations are developed in the litterature for predicting mean flow velocity for example on a wide range of in situ river flow measurements in [46] or else for gravel bed streams in [47]. The friction depends on the flow depth through the proposed power law relation (Eq. 2) enabling a variation of the friction effect in function of the flow regime for complex flow zones for instance; this spatially distributed friction law is richer than a constant uniform value as it is often set in the literature from a-priori tables of frictions in function of river types for instance (e.g. [48]).

Note that satellite altimetry mostly observes the downstream parts of river networks (top width $W > 100$m for SWOT), mainly in subcritical and mostly low Froude flows at the observation scales (cf. [49, 1, 3]). The discharge $Q_{in}(t)$ is classically imposed upstream of the river channel with a discharge hydrograph. At downstream a normal depth is imposed using the Manning-Strickler equation depending on the unknowns $(A, Q; K)_{out}$ (it is classically integrated in the Preissmann scheme equations). The initial condition is set as the steady state backwater curve profile $Z_0(x) = Z(Q_{in}(t_0))$; also depending on the unknowns. Note that these boundary and initial conditions are updated during the iterative inverse method presented in what follows. This 1D Saint-Venant model (Eq. 1)

is discretized using the classical implicit Preissmann scheme (see e.g. 50) on a regular grid of spacing Δx. It is implemented into the computational software DassFlow (DassFlow [51]).

2.2. Effective anabranching river model from multisatellite data

A $L = 71$km long portion of the Rio Xingu containing anabranching reaches is considered (Fig. 1, cf. [2],). WS observations are available at 6 virtual stations along a single ENVISAT track (#263) representing 77 samples of WS profiles between mid 2002 and mid 2010 (cf. [17]); that is $\left\{Z_{s,p}^{obs}\right\}_{S,P}^{env}$ with $S = 6$ corresponding to the locations of the virtual stations simultaneously observed at $P = 77$ times (see Tab. 1).

An effective hydraulic modeling strategy of this anabranching river is proposed based on:

- Cross-sectional water surface widths $\{W\}_{S,2}^{jers}$ obtained from JERS mosaics (Courtesy of GRFM, NASDA/MITI) in low and high flows. The effective water surface width is the sum of the width of all individual river channels for anabranching reaches. Note that the cross section geometry of this (ungauged) anabranching river might be changing over a hydrological year, from "disconnected channels" in low-flows to a "mono-channel" with forested floodplains during the flood season. The available satellite images resulted in an estimation of a larger effective top width in high-flow.

- An a priori river bottom $\{b\}_{rvs}$ obtained from altimetric rating curves from [52]. The authors determined effective bottom elevations by adjusting the scalar parameters γ and δ of a classical stage discharge relationship $Q = \gamma(Z - b)^{\delta} I^{1/2}$, with I the water surface slope gained from altimetry at large scale. They used WS elevations gained by satellite altimetry and discharges simulated with the large scale hydrological model MGB ([53, 54, 55]) on the temporal window of interest - called true discharge in what follows.

Effective cross-sections geometries are defined at the 6 virtual stations with the bathymetry b given by altimetric rating curves and from effective widths such that low flow width (resp. high flow) is reached for the first (resp. ninth) decile of observed WS elevations for each cross section. The final model geometry is obtained by linear interpolation between these 6 effective cross sections on the model grid with $\Delta x = 50m$. It is shown in Fig. 1 along with ENVISAT and SWOT spatial samplings. The friction law (Eq. 2) introduced above and depending on the flow depth h is distributed using patches with constant values for each reach between two successive virtual stations.

2.3. The computational inverse method

This paper investigates the estimation of the hydraulic triplet ($Q(t)$, $b(x)$, $K(x,h)$) from observations of WS variabilities only on an anabranching river. The employed inverse method is those presented in [1] (see also [36]) with an augmented composite control vector c; it is detailed in Appendix 7. c contains a spatially distributed friction coefficient enabling to model complex flow zones (while it is an uniform friction law $K(h)$ in [1]). This definition of $K(x,h)$ enables to consider more heterogeneous bathymetry controls.

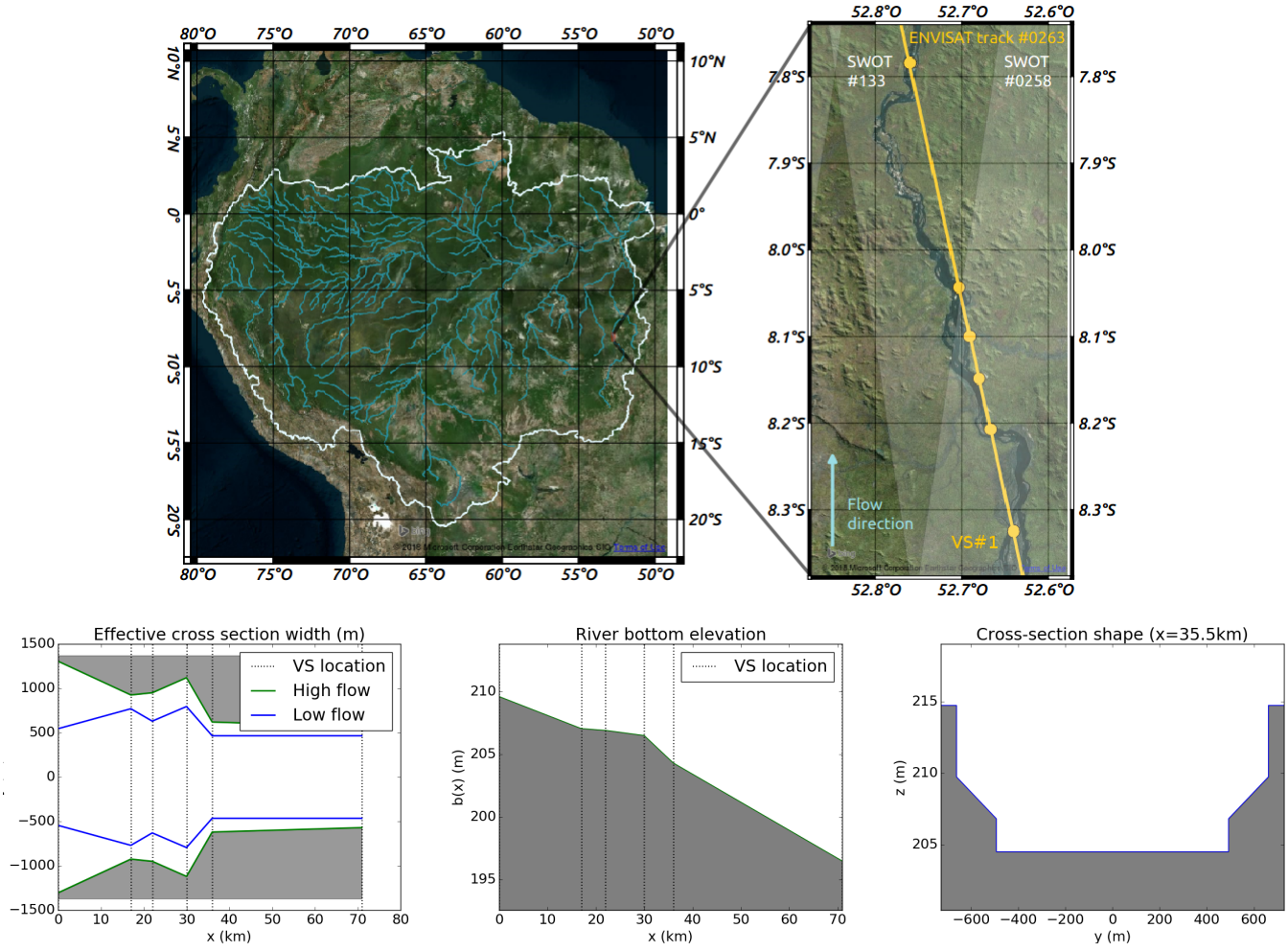

Figure 1: Study zone (top) with ENVISAT track #263 and virtual stations (orange dots); simulated SWOT tracks #133 and #258 on the 1^{st} and 6^{th} day every 21 days repeat cycle (transparent white). Effective river bathymetry derived from altimetric rating curves ([52]) and water surface width from satellite images.

The principle is to estimate (discrete) flow controls minimizing the discrepancy between Z_{obs} the observed flow line and Z the modeled one; the latter depending on the unknown parameters vector c through the hydrodynamic model (Eq. 1). This discrepancy is quantified through the cost function term:

$$j_{obs}(c) = \frac{1}{2}\|Z_{obs} - Z(c)\|_2^2 \tag{3}$$

see Appendix 7 for details. The control vector c contains the unknown "input parameters" of the 1D Saint-Venant shallow water flow model (Eq. 1) considering effective cross sections (see Fig. 1). In the present study, c reads as:

$$c = (Q_{in,0},\ ...,\ Q_{in,P};\ b_1,\ ...,\ b_R;\ \alpha_1,\ ...,\alpha_N,\ \beta_1,\ ...,\beta_N)^T \tag{4}$$

where temporally and spatially distributed controls are the upstream discharge $Q_{in,p}$, the river bed elevation b_r and the distributed friction parameters α_n and β_n.

The subscript p denotes the observation time $p \in [0..P]$ and r denotes the reach number, $r \in [1..R]$.

α_n and β_n are the parameters of the friction law depending on the model state h (Eq. 2) for each patch $n \in [1..N]$ with $N \leq R$.

The inversion consists to solve the following minimization problem: $c^* = \text{argmin j}(c)$ (Eq. 9).

This minimization, optimization problem is solved using a first order gradient-based algorithm, more precisely the classical L-BFGS quasi-Newton algorithm. The main steps of the method are illustrated in Fig. 2.

3. Model Calibration

This section presents the calibration of the effective hydraulic model based on the reference effective geometry defined above (cf. section 2.2). The observed water elevation time series $\left\{Z_{s,p}^{obs}\right\}_{S,P}^{env}$ at $S = 5$ ENVISAT virtual stations are used to calibrate the friction law of the 1D Saint-Venant flow model (Eq. 1). Since friction has a local and upstream influence on a flow line (low Froude fluvial flows, Fig. 10) the remaining ENVISAT time series at VS#6 downstream of the river domain will be used for infering the full control vector c in next section - recall that a normal depth is used as downstream BC (cf. section 2.1).

A "reduced" control vector $c_{cal} = (\alpha_1,\ ...,\alpha_N,\ \beta_1,\ ...,\beta_N)$ consisting in spatially distributed friction parameters only is considered here. In order to avoid a spatial "overparameterization" regarding the 5 water height timeseries available at VS, the choice is made to spatialize friction on $N = 5$ patches, on each reach downstream an altimetric VS. The inverse method presented in [1] and described in appendix (section 7) is used here with no regularization nor variable change for this "simple" calibration problem.

An optimal friction distribution c_{cal}^* is found with the inverse method and the calibrated values of $\alpha_{n=1...5}$ and $\beta_{n=1...5}$ are summed up in Tab. 1. The resulting water height time series are compared to altimetric observations

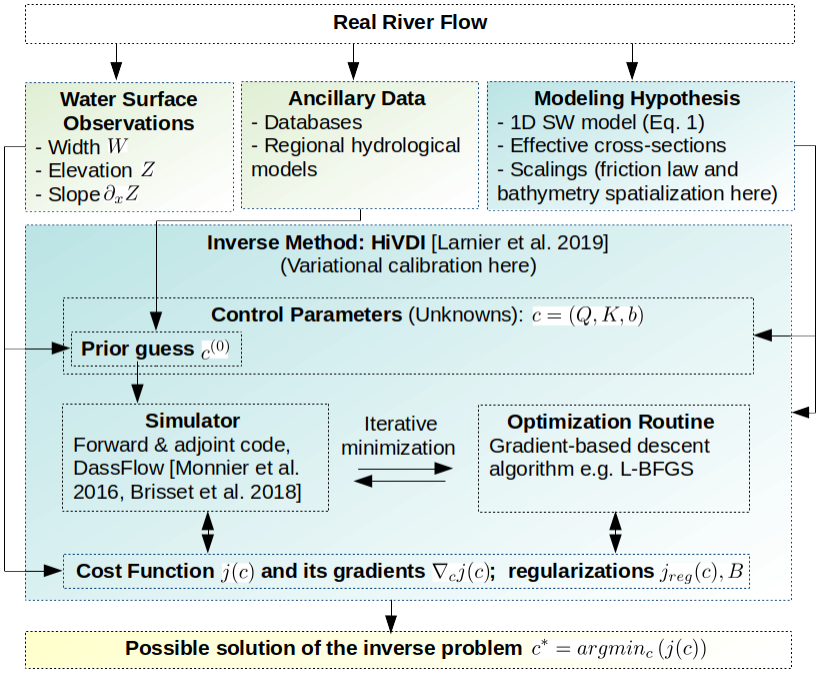

Figure 2: Flowchart of the method using the HiVDI inverse method (Larnier et al. [1]) for variationnal calibration, adapted from Monnier et al. [56], Monnier [57].

for each virtual station (cf. Fig. 3). The spatially distributed friction law (Eq. 2) enables a fairly good reproduction of the observed water level variations on this anabranching river, across a wide range of flows, even with an effective 1D model built on multi-satellite data (Fig. 3).

A constant friction in time would lead to systematical errors for a large range of flows as shown by the grey curves on Fig. 3. The calibrated friction exponents β_n range between 0.482 and 1.133 except for the second reach (SV2-3) where a small β_n is found, that is a barely constant friction across flow regimes for this short reach (cf. Fig. 3). The spatial pattern of α_n values calibrated here corresponds to significant friction effects, varying across flow regimes, and necessary to effectively represent anabranching reaches using a 1D effective cross section. Indeed the lattest leads to an underestimation of the hydraulic radius $R_h = {}^{A}/_{P_h}$ hence of the friction slope $S_f = {}^{|Q|Q}/_{K^2 A^2 R_h^{4/3}}$ in the 1D Saint-Venant model (see section 2.1) for anabranching reaches.

4. Inferences of distributed spatio-temporal flow controls $(Q(t), K(x,h), b(x))$ from WS observations

This section studies the challenging inference of the hydraulic triplet (discharge, bathymetry, friction) from multi-satellite WS observations. The anabranching Xingu River morphology represents a supplementary difficulty for inversions regarding the variability of local hydraulic behaviors accross flow regimes as evidenced above by the calibrated friction laws ($\beta^{cal} \neq 0$). The impact of spatial controls density and bathymetry representation is

Virtual station name	VS#1	VS#2	VS#3	VS#4	VS#5	VS#6
Flow distance to mouth [km]	1146	1129	1124	1116	1110	1075
Flow distance from the upstream [km]	0	17	22	30	36	71
Drainage area [km^2] (MGB model)	193.255	193.255	194.148	194.148	195.882	197.862
Z_0 [m] (reference : EGM2008) (Paris et al. 2016)	209.6	207.1	206.9	206.5	204.3	196.5
$W_{low}(x)$ Total low flow width [m] (derived from JERS)	1090	1540	1260	1590	930	930
$W_{high}(x)$ Total high flow width [m] (derived from JERS)	2610	1850	1900	2240	1240	1140
Calibrated friction factor $\alpha^{cal}(x)$ (downstream reach)	12.785	19.574	9.869	4.252	7.425	-
Calibrated friction exponent $\beta^{cal}(x)$ (downstream reach)	0.482	0.071	0.624	1.133	0.718	-

Table 1: Summary of the effective hydraulic model parameters including calibrated friction parameters $\alpha^{cal}(x)$ and $\beta^{cal}(x)$ (recall $K(x,h) = \alpha(x)h^{\beta(x)}$) using 8 years of WS elevation variations (ENVISAT data) given effective channel bathymetry and upstream discharge from the MGB hydrological model ([54]).

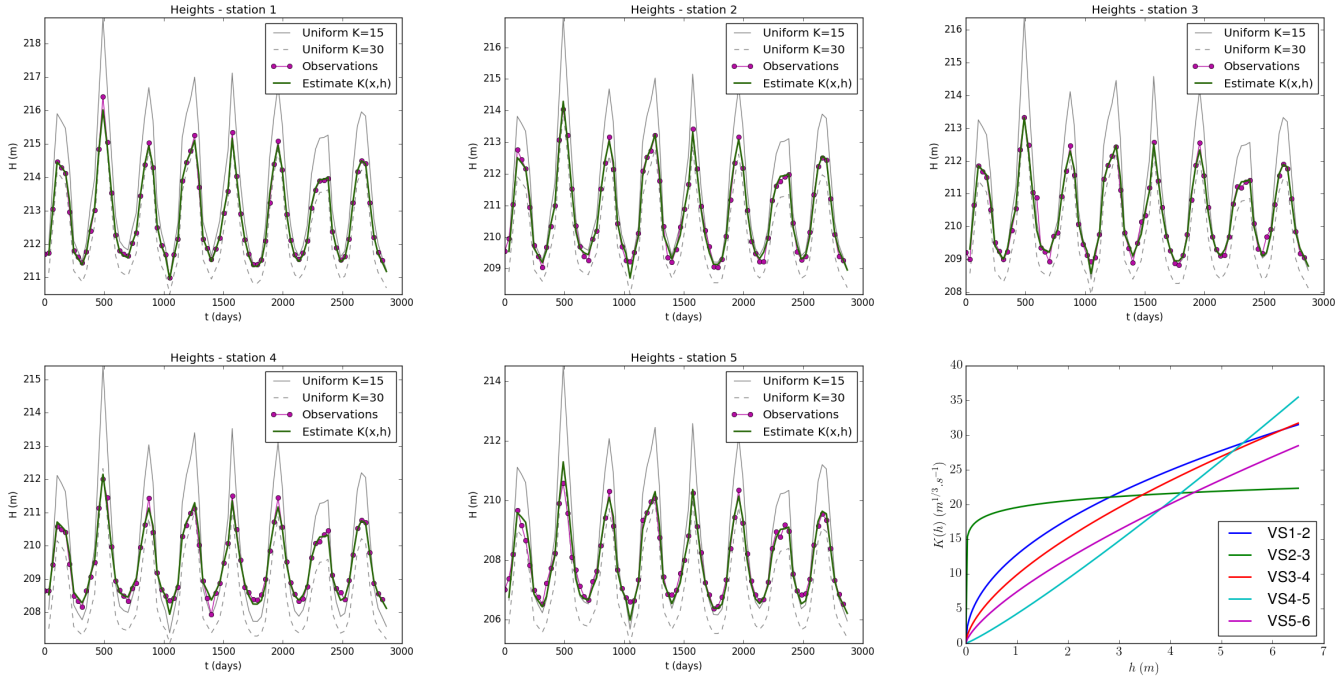

Figure 3: Calibration of variable friction $K(x,h)$ with 8 years of ENVISAT measurements at 6 VS using the variational method with $c = (\alpha_1, ..., \alpha_5, \beta_1, ..., \beta_5)$; $j_{obs} = 0.07$. (Bottom right) Effective friction law in function of water depth for each VS.

asssessed in what follows regarding the spatial sparsity of observations. First is presented the numerical experiment framework, then the inferences with relatively "sparse" ENVISAT measurements and finally those with SWOT synthetic observations.

4.1. Design of the numerical experiments

The effective hydraulic model described in section 2.2 and calibrated in section 3 is used as a reference ("*target*") in the following numerical experiments. The control vector (Eq. 4) containing discharge, bathymetry and friction is sought with the inverse method decsribed in section 2.3 (see also appendix, section 7). It is tested first with real ENVISAT time series repesenting a relatively sparse spatial sampling of WS signatures with 6 VS on this $71km$ long river, and next with synthetic SWOT observations sampling the flow line at $\Delta x = 200m$ (RiverObs product, see [58]).

The Xingu River is observed either by a single along-stream ENVISAT track at 6 observation points (virtual stations) of flow lines every 35 days, or two SWOT tracks providing dense WS observations in space twice per 21 days repeat cycle (5 days delay, cf. section 2.2). Note that the temporal sparsity of observations (35 days for ENVISAT or 5 days between the two SWOT passes every 21 days) only enables to identify low hydrograph frequencies, at observation times (see [36] for a detailled analysis and the identifiability maps). Indeed the hydraulic wave propagation time is around $T_{wave} \sim 9h$ which is much smaller than the lowest satellite revisit time of 5 days. This propagation time is calculated using the kinematic wave velocity for rectangular channels $c_k = 5/3U$ and maximal high flow velocity $U = 2.17$m/s from calibrated model outputs $c_k = 2.2$m/s (second hydrograph peak at $t = 490\,days$, see flow variables on Fig. 10). Let $I_{indent} = T_{wave}/\Delta t_{obs}$ be the identifiability index defined in [36] as the ratio between flood wave propagation time and observation time step. This leads to a very low temporal identifiability index for this $71km$ river: $I_{ident} = 7.5 \times 10^{-2}$ for SWOT and $I_{ident} = 10^{-2}$ for ENVISAT. Consequently, only low temporal dynamics and discharge at observation times are inferable as shown in [36]; SWOT and ENVISAT observations are thus considered separately in the present study.

The starting point of the VDA process in the parameter space, the so-called prior c_{prior} (cf. section 7), consists in a rough hydrological prior: $Q^{(0)} = \overline{Q}_{MGB}$ the mean discharge estimated from the MGB hydrological model, a spatially constant $\alpha^{(0)}$ friction defined a priori from classical hydraulic ranges (e.g. [48]) and $\beta^{(0)} = 1$, the bathymetry $b^{(0)}$ is defined as a simple straight line over the whole domain for hydraulic analysis first. Note that the sensitivity of the inference to the prior definition is investigated in section 5.

In a noised observation context, we denote by δ the noise level such that $\|Z_{obs} - Z_{true}\|^2 \leq \delta$ for all spatial locations r with Z_r^{obs} the observed and Z_r^{true} the true WS elevation. A common technique to avoid overfitting noisy data, in the context of Tykhonov's regularization of ill-posed problems, is Morozov's discrepancy principle, (see e.g. [59] and references therein): the regularization parameter γ (see Eq. 7) is chosen *a-posteriori* such that j does not decrease below the noise level. In the present numerical experiments, the convergence is stopped if $j_{obs}(c) \leq 10^{-1}$ or if j_{obs} is not decreased anymore for higher discrepencies.

4.2. Inference from spatially sparse ENVISAT snapshots

In this section the assimilation is based on WS elevations $\left\{Z_{s,p}^{env}\right\}_{S,P}$ at $S = 6$ virtual stations observed simultaneously by ENVISAT during 8 years every 35 days, i.e. $P = 77$. In this spatially sparse observation context, the impact of spatial controls density is investigated.

First, we consider a "full" control vector c (cf. Eq. 4) including $P = 77$ inflow discharges, all 1D model bathymetry points $R = 1420$ and $N = 5$ friction patches between ENVISAT virtual stations (cf. section 2.2). The infered inflow discharge, bathymetry and friction are presented in Fig. 4 (case Env.a). Despite the satisfying value of the hydraulic controls reached at iteration 35, the descent is still possible as shown by j_{obs} decreasing of about 20% at iteration 96. Allthough it enables to fit the observations according to the a priori convergence criteria defined in section 4.1, the solution found after the VDA process is not very accurate nor realistic as shown by peak flow underestimations and significant oscillations of the identified friction and bathymetry. The spatial sparsity of observations prevents to infer these relatively dense bathymetry controls; in this case the considered inverse problem is underconstrained.

In order to better constrain the inverse problem in case of sparse spatial observability, a bathymetry representation is consistently introduced at the scale of the observation grid and applied to the finer flow modeling grid. Based on the physical analysis of the SW model (Eq. 1) behaviour and the WS signature of bathymetry/friction controls (see [20, 60, 3]), a linear bathymetry interpolation is used between the successive couples of bathymetry controls defined at observation points only. The resulting bathymetry $\tilde{b}(x) \in \mathcal{C}^0(\mathbb{R}), \forall x \in [0, L]$ is piecewise linear and strongly constrains the bathymetry profile between the sought bathymetry points - instead of using only a weak constraint $j_{reg}(c) = \frac{1}{2} \left\| b"(x) \right\|_2^2$ in the optimization process (cf. appendix 7) as done in the next section 4.3 with spatially dense SWOT observations. Using this bathymetry constraint with $R = 6$ bathymetry controls defined at each ENVISAT virtual station results in 5 reaches and $N = 5$ friction patches are consistently applied to each. This leads to a more robust and accurate inference as shown in Fig. 5 (case Env.b). The discharge infered for 8 years is fairly correct (RMSE $= 520\,\mathrm{m}^3/\mathrm{s}$, Nash $= 0.95$) and relatively realistic bathymetry/friction patterns are found, with some compensations between spatial controls locally in space, which is further analyzed in what follows.

The impact, on the infered parameters, of searching a spatially uniform friction law is tested with the piecewise linear bathymetry representation used above. The resulting discharge inference is fairly correct (RMSE $= 608\,\mathrm{m}^3/\mathrm{s}$, Nash $= 0.93$) and interestingly the bathymetry spatial pattern is well retrieved but shifted above the reference one (cf. Fig. 6) (case Env.c). The infered friction coefficients are $\alpha = 22.621$, $\beta = 0.217$, which represents a lower friction effect on most flow regimes regarding the calibrated ones (cf. Tab. 1). These infered effective friction law and bathymetry patterns, leading to somehow effective stage-discharge relationships locally given the infered hydrograph and its propagation, enable to approximate the observed WS variations ($j_{obs} = 1.269$) but with a less accurate fit than with spatially distributed friction ($j_{obs} = 0.118$). Note that in this case of lower model complexity an underestimation of the low flow discharges occurs.

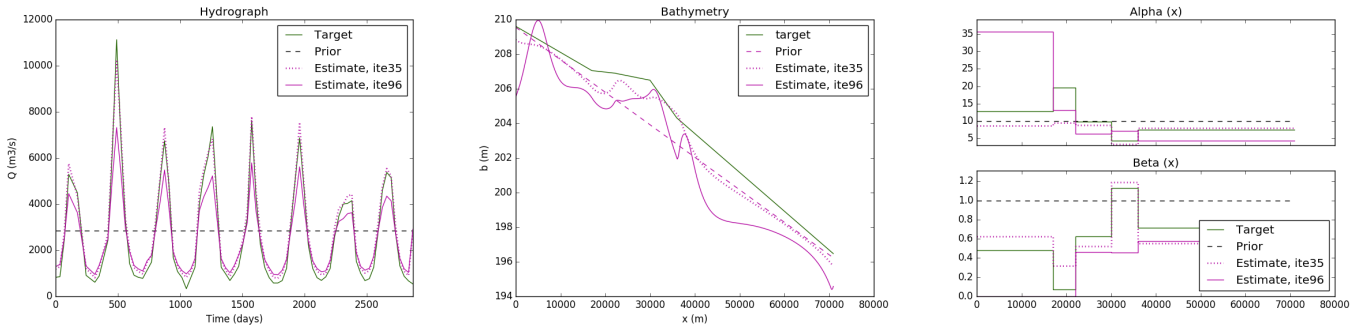

Figure 4: Identification of $(Q(t), K(x,h), b(x))$ with ENVISAT observations and overparameterized $c = \left(Q_{in,0}, ..., Q_{in,P}; b_1, ..., b_R; \alpha_1, ..., \alpha_N, \beta_1, ..., \beta_N\right)^T$ with $P = 77$, $R = 1420$, $N = 5$, bathymetry regularization weight $\gamma = 10^{-3}$; $j_{obs} = 0.098$ at iteration 35 (top) and $j_{obs} = 0.077$ at iteration 96 (bottom) (Env.a)

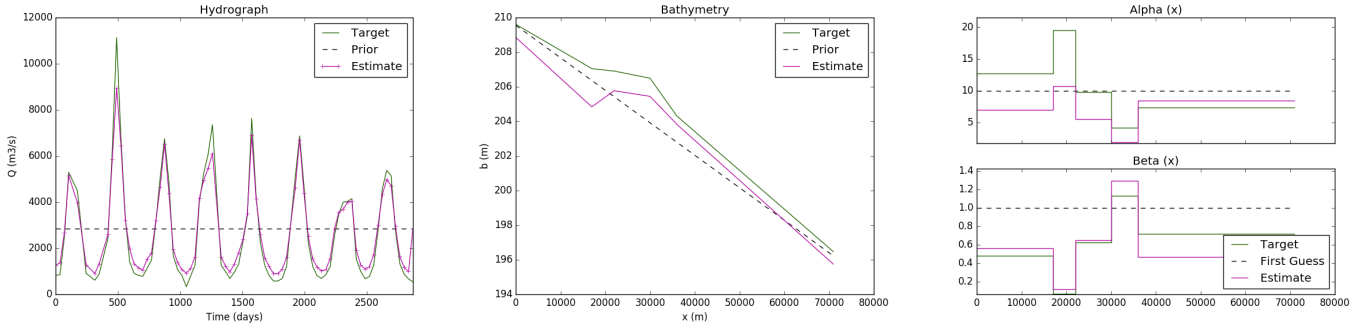

Figure 5: Identification of $(Q(t), K(x,h), b(x))$ with ENVISAT observations and effective $c = \left(Q_{in,0}, ..., Q_{in,P}; b_1, ..., b_R; \alpha_1, ..., \alpha_N, \beta_1, ..., \beta_N\right)^T$ with $P = 77$, $R = 6$, $N = 5$ with a piecewise linear bathymetry $b(x)$ reconstruction, $\gamma = 0$; $j_{obs} = 0.118$ at iteration 51. (Env.b)

Recall that the observations consist in real measurements of WS elevations gained by nadir altimetry on anabranching reaches of the Xingu River. The complexity of the forward-inverse modeling approach, in coherence with the spatial sparsity of the observation grid, enables to approximate satisfactorily the one of the observed anabranching flow. The additionnal constraint provided by spatially dense flow lines observations is investigated in the next section with SWOT synthetic data.

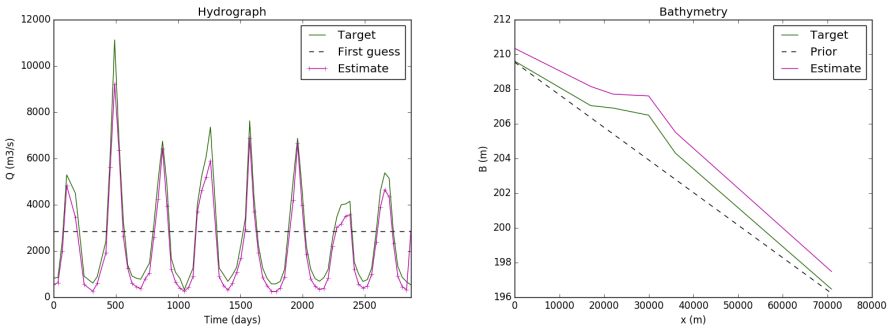

Figure 6: Inferrence of $Q(t)$, $b(x)$ and spatially uniform $K(h) = \alpha h^{\beta}$ with ENVISAT WS observations and effective $c = \left(Q_{in,0}, ..., Q_{in,P}; b_1, ..., b_R; \alpha, \beta\right)^T$, $P = 77$, $R = 6$, no bathy $\gamma = 0$; $j_{obs} = 1.269$ at iteration 54. The identified friction coefficients are $\alpha = 22.621$, $\beta = 0.217$. (Env.c)

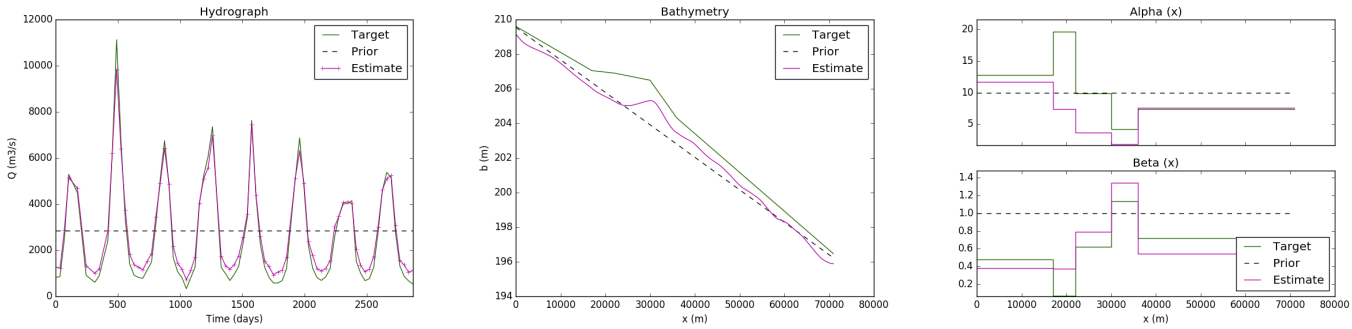

Figure 7: Identification of $(Q(t), K(x, h(x,t)), b(x))$ with SWOT-sge observations and effective $c = \left(Q_{in,0}, ..., Q_{in,P}; b_1, ..., b_R; \alpha_1, ..., \alpha_N, \beta_1, ..., \beta_N\right)^T$ with $P = 276$, $R = 1420$, $N = 1419$, $\gamma = 10^{-3}$; $j_{obs} = 0.099$ at iteration 41. (SWOT.a)

4.3. Inference from spatially dense SWOT snapshots

In this section the full hydraulic control c (cf. Eq. 4) is infered by assimilating SWOT-like observations. Those noisy data are computed using the SWOT hydrology simulator applied to flow lines from the effective hydraulic model calibrated above (cf. section 3). The SWOT spatio-temporal pattern over the studied river is obtained by overlapping the river centerline and the expected SWOT orbit and swaths (cf. Fig. 1). Finally the synthetic SWOT-like observables consist in WS elevations $\left\{Z_{obs}^{SWOT}\right\}_{r,p}$ with $p \in [1..P]$ and $P = 276$ generated on the fine scale model grid i.e. $r \in [1..1420]$.

The inflow discharge, bathymetry and friction are infered by assimilating SWOT WS observations $\left\{Z_{obs}^{SWOT}\right\}_{r,p}$ on the same spatial grid as that of the numerical hydraulic model with c_{prior1}. The estimates are presented on Fig. (7). The infered discharge hydrograph is accurate (RMSE $= 391\,\mathrm{m}^3/\mathrm{s}$, Nash $= 0.97$) and bathymetry/friction patterns are relatively well retrieved. Using SWOT spatially distributed observations and piecewise constant friction enable to constrain the inference of bathymetry controls at a fine spatial resolution (model grid). The inverse method includes: (i) a regularization term j_{reg} in the cost function (Eq. 7); (ii) covariance matrices acting as spatial or temporal smoothers/regularizations (cf. Eq. 12 in appendix). The infered discharge and spatially distributed controls are slightly more accurate than previously in a comparable inversion scenario with sparse ENVISAT observations in space and piecewise linear bathymetry constrain (case Env.b, cf. Tab. 2 and Fig. 5). Note that the friction is sought by reaches which enables to consider more dense bathymetry controls. Again, the compensation between spatial controls appears locally in space but enables the best fit to the distributed measurements of WS elevations given the infered discharge ($j_{obs} = 0.099$).

5. Discussion and numerical investigation of the bathymetry-friction equifinality

This section discusses the challenging inference of spatially and temporally distributed river flow controls from water surface observations through numerical investigations. Indeed, the considered flow controls ($Q(t)$, $b(x)$,

$K(x,h)$) have a correlated influence and can produce undiscernable signatures in the modeled flow lines therefore leading to an ill-posed inverse problem (cf. [27, 1] for investigations on this "*bathymetry-friction equifinality*" in a comparable data-inversion context). The hydrograph is responsible for flow variability in time, hence enabling to retrieve the temporal dynamics of the observed flow lines [36, 1].

Given altimetric measurements of WS variabilities and the first guess c_{prior1}, the regularized inverse method enables to infer a complex control vector composed of temporally and spatially distributed controls of the 1D SW model (Eq. 1). In the numerical experiments above, the discharge hydrograph $Q(t)$ is accurately infered at observation times but because of the ill-posedness of the inverse problem, compensations can occur between the sought parameters and especially between the spatial controls - the bathymetry $b(x)$ and the distributed friction parameters $\alpha(x)$ and $\beta(x)$. These infered friction laws and bathymetry patterns - simultaneously infered with the discharge hydrograph - correspond to "effective rivers" enabling to fit the observed variability of flow lines.

Note that the spatial density of SWOT data enables to constrain flow controls that are relatively dense in space, here on a complex anabranching flow case using the effective 1D river representation and a friction law pattern depending on water depth. Improving the physical segmentation, parameterization and sparse representation of river networks and flow signatures (e.g. [3]) seems of great importance to take advantage of the forthcoming SWOT observations along with other data.

Importantly, as already pointed out in the VDA inferences performed with the DassFlow model using SWOT like data in [36, 1] and AirSWOT data in [40], the accuracy of the inferred discharge depends on the quality of the prior. In other words spatially distributed WS observations enable to depict spatio-temporal signatures and eventually propagation dynamics but a *quantitative biais* remains regarding fluxes, from the river reach to the network scale.

In the following subsection the influence of the prior value on the quality of the inferences with spatially distributed controls is investigated first. Next, is proposed a numerical analysis of the sensitivity of the friction slope (source term) S_f in the Saint-Venant equations (Eq. 1) to the flow controls (triplet) that are embeded in it (Manning-Strickler parameterization).

5.1. Sensitivity to the prior guess

The sensitivity of the inference to the quality of the prior guess of the control vector c_{prior} is investigated here for the most challenging inverse problem with spatially and temporally distributed controls and sparse ENVISAT data. First the inflow prior is varied of $\pm 30\%$ around the mean true discharge; the river bottom elevation and friction priors are set as previously in c_{prior1}. The infered hydraulic controls are presented in Fig. 8 and various inference scores are summed up in Tab. 2. For each inflow prior, the temporal variations of the inflow hydrograph are very well retrieved as shown on Fig. 8 - runs Env.b2 and Env.b3. However a biased inflow prior results in a biased hydrograph estimate (with correct temporal variations at observation times) which is coherent with results of [1, 40]).

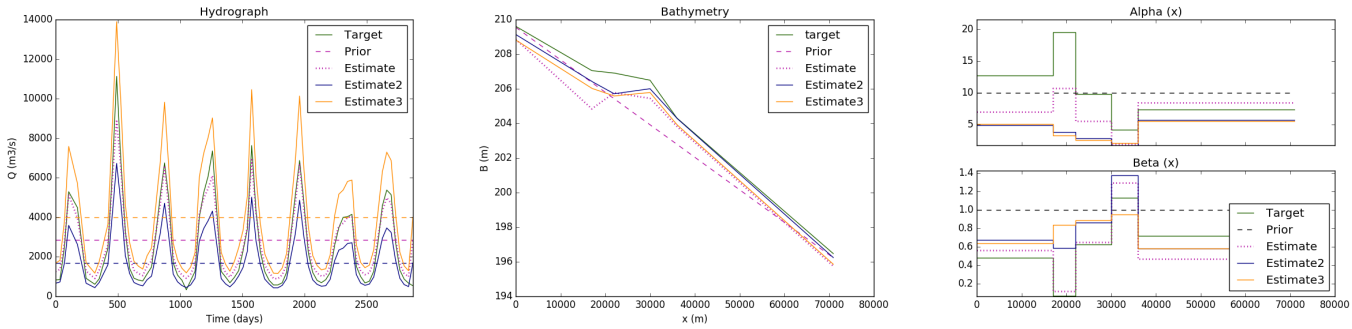

Figure 8: Sensitivity test to the prior discharge $\overline{Q_{MGB}} \pm 30\%$; identification (var change) of $(Q(t), K(x,h), b(x))$ with ENVISAT observations $c = \left(Q_{in,0},\ ...,\ Q_{in,P};\ b_1,\ ...,\ b_R;\ \alpha_1,\ ...,\alpha_S,\ \beta_1,\ ...,\beta_S\right)^T$ with $P = 77$, $R = 6$, $N = 5$ and with a piecewise linear $b(x)$ and $S = R = 5$. "Estimate" (case Env.b) $j_{obs} = 0.118$ at iteration 51, "Estimate2" (case Env.b21) $j_{obs} = 0.125$ at iteration 41, "Estimate3" (case Env.b21) $j_{obs} = 0.125$ at iteration 25.

Next, the sensitivity to the prior bathymetry and friction is tested. The prior bathymetry is infered with the low-complexity system proposed in the hierarchichal HiVDI model chain ([1]) for ungauged rivers. It consists in estimating an effective prior bathymetry from WS observables using the low Froude model and prior discharge from a hydrological model ($\overline{Q_{MGB}}$ here) and prior friction $(\alpha^{(0)}, \beta^{(0)})$. Two prior guesses c_{man1} and c_{man2} are considered with prior friction under/over-estimations compared to calibrated ones (cf. Fig. 9). As shown on Fig. 9, the inference in case Env.b31 (blue) results in an accurate estimation of discharge, very similar to Env.b (purple). It is started from a prior guess c_{man1} that underestimates river bottom elevation and overestimates the spatially averaged friction effect compared to calibrated values (cf. Fig. 9, bottom). In that case, fitting WS elevations enables to infer an effective river channel (bathymetry and friction) but also to infer a fairly realistic upstream temporal control (discharge hydrograph). Using the prior guess c_{man2} that overestimates both river bottom elevation and spatially averaged friction effect results in a comparable fit to the observed WS elevations. However this correct fit stems from the compensation between an infered effective channel of reduced conveyance capacity (comparable friction effects but overestimated bed levels) and consequently an infered hydrograph with underestimated low-flow discharges (in yellow).

5.2. Spatio-temporal sensitivity of the friction term

The considered flow controls ($Q(t)$, $K(x,h)$, $b(x)$) of the 1D Saint-Venant shallow water equations (Eq. 1) have a complex non linear influence on the modeled flow lines and consequently on the fit to the observed ones - the lattest being evaluated globally in space and time with the current inverse method given the observation cost function (Eq. 3). The variation of momentum expressed by the second flow equation is due to a pressure source term $-gA\,\partial_x Z$ (including the longitudinal variation of fluid-to-fluid pressure, the longitudinal variation of lateral

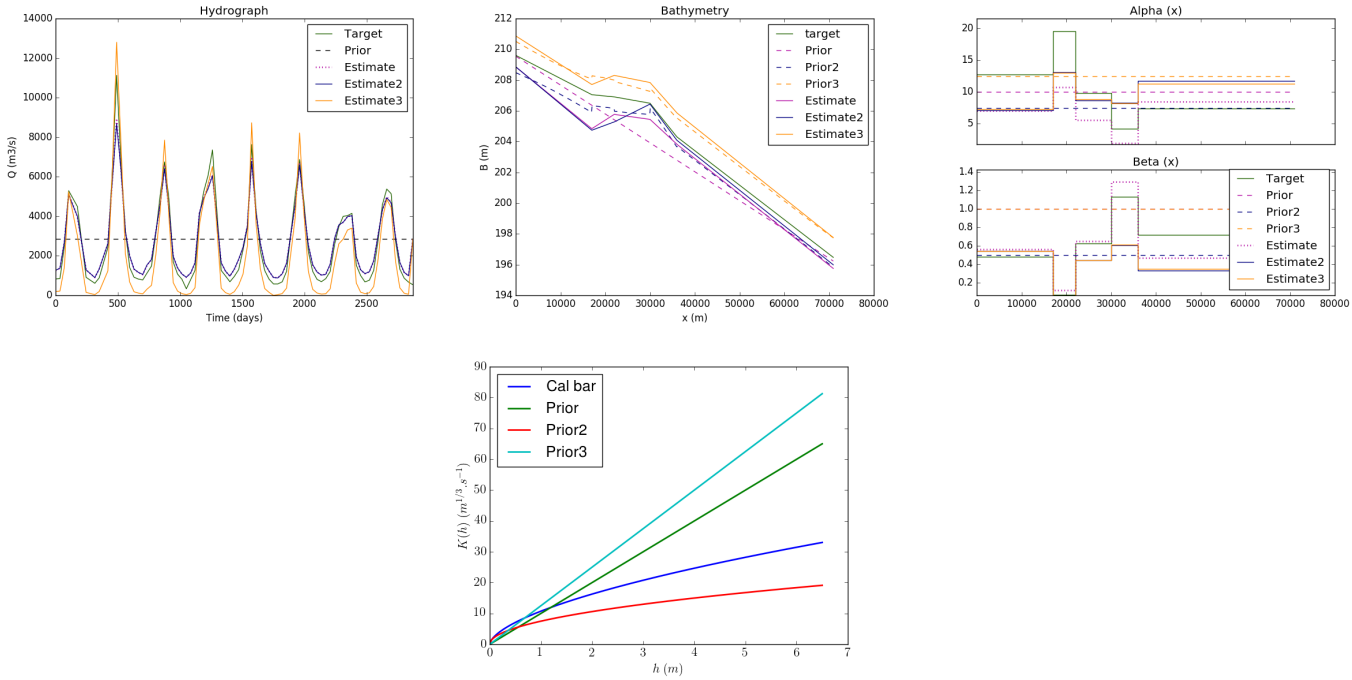

Figure 9: Sensitivity test to the prior friction and bathymetry estimated using the "Manning" method from [1] (c_{man1} ($\alpha^{(0)} = 7.5$; $\beta^{(0)} = 0.5$) and c_{man2} ($\alpha^{(0)} = 12.5$; $\beta^{(0)} = 1$)); identification (var change) of $(Q(t), K(x,h), b(x))$ with ENVISAT observations $c = \left(Q_{in,0}, ..., Q_{in,P}; b_1, ..., b_R; \alpha_1, ..., \alpha_S, \beta_1, ..., \beta_S\right)^T$ with $P = 77$, $R = 6$, $N = 5$ and with a piecewise linear b(x) and $S = R = 5$. "Estimate" (case Env.b) $j_{obs} = 0.118$ at iteration 51, "Estimate2" (case Env.b31) $j_{obs} = 0.116$ at iteration 46, "Estimate3" (case Env.b32) $j_{obs} = 0.122$ at iteration 41. (Bottom) prior effective friction laws and spatially averaged calibrated friciton law ($\overline{\alpha_{cal}} = 10.74$ and $\overline{\beta_{cal}} = 0.6$, "Cal bar").

Case	Control	Prior	$\text{RMSE}_{Q^{(0)}}$ (m^3/s)	$r\text{RMSE}_{Q^{(0)}}$ (%)	$\text{Nash}_{Q^{(0)}}$ $(-)$	$\text{RMSE}_{b^{(0)}}$ (m)	$\text{RMSE}_{\alpha^{(0)}}$ $(m^{1/3-\beta}/s)$	$\text{RMSE}_{\beta^{(0)}}$ $(-)$
Env.a	Dense $b(x)$	c_{prior1}	2254	194	-0.01	1.19	4.93	0.49
Env.b	Piec. $b(x)$	c_{prior1}	"	"	"	"	"	"
Env.c	Piec. $b(x)$, $K(h)$	c_{prior1}	"	"	"	"	"	"
SWOT.a	Dense $b(x)$	c_{prior1}	"	"	"	"	"	"
Env.b21	Piec. $b(x)$	$Q^{(0)}_{prior1} - 30\%$	2433	97	0.18	1.19	4.93	0.49
Env.b22	Piec. $b(x)$	$Q^{(0)}_{prior1} + 30\%$	2626	297	-0.37	"	"	"
Env.b31	Piec. $b(x)$	c_{man1} ($\alpha^{(0)} = 7.5$; $\beta^{(0)} = 0.5$)	2254	194	-0.01	0.77	5.63	0.34
Env.d32	Piec. $b(x)$	c_{man2} ($\alpha^{(0)} = 12.5$; $\beta^{(0)} = 1$)	2254	194	-0.01	1.13	5.43	0.49

Case	Control	Prior	RMSE_Q (m^3/s)	rRMSE_Q (%)	Nash_Q $(-)$	RMSE_b (m)	RMSE_α $(m^{1/3-\beta}/s)$	RMSE_β $(-)$
Env.a	Dense $b(x)$	c_{prior1}	830	57	0.86	1.97	10	0.46
Env.b	Piec. $b(x)$	c_{prior1}	520	61	0.95	1.07	4.8	0.37
Env.c	Piec. $b(x)$, $K(h)$	c_{prior1}	608	58	0.93	1.05	–	–
SWOT.a	Dense $b(x)$	c_{prior1}	391	38	0.97	0.91	5.67	0.2
Env.b2	Piec. $b(x)$	$Q^{(0)}_{prior1} - 30\%$	1229	39	0.7	0.48	7.83	0.28
Env.b3	Piec. $b(x)$	$Q^{(0)}_{prior1} + 30\%$	1473	104	0.57	0.75	5.09	0.22
Env.bm2	Piec. $b(x)$	c_{man1} ($\alpha^{(0)} = 7.5$; $\beta^{(0)} = 0.5$)	550	61	0.94	1.22	4.64	0.32
Env.bm3	Piec. $b(x)$	c_{man2} ($\alpha^{(0)} = 12.5$; $\beta^{(0)} = 1$)	885	78	0.84	1.30	5.50	0.35

Table 2: Scores of the inferences (bottom) performed with various priors (top), ENVISAT ("Env") or SWOT ("SWOT") observations.

and bottom wall-to-fluid pressure) and a dissipation term $-gAS_f$. The discharge and the bathymetry appear in the momentum and pressure terms while all the flow controls are embedded in the friction source term S_f. Note that for a locally steady uniform flow $S_f = -\partial_x Z$ and an infinity of friction and bathymetry values can correspond to a single value of discharge (cf. Garambois and Monnier [27], Larnier et al. [1]).

We propose a simple calculation in order to make appear the sensitivity of the friction term to a change on the controls; let us express the differential of S_f assuming $Q > 0$:

$$\begin{aligned} \mathrm{d}S_f &= \mathrm{d}\left(\frac{1}{K^2}\frac{Q^2}{A^2 R_h^{4/3}}\right) \\ &= -\frac{2}{K^3}\frac{Q^2}{A^2 R_h^{4/3}}\mathrm{d}K - \frac{2}{A^3}\frac{Q^2}{K^2 R_h^{4/3}}\mathrm{d}A - \frac{4}{3R_h^{7/3}}\frac{Q^2}{K^2 A^2}\mathrm{d}R_h + \frac{1}{K^2}\frac{2Q}{A^2 R_h^{4/3}}\mathrm{d}Q \end{aligned} \tag{5}$$

Since $\mathrm{d}R_h = \mathrm{d}(A/P) = \frac{1}{P}\mathrm{d}A - \frac{A}{P^2}\mathrm{d}P = \frac{1}{P}\left(\mathrm{d}A - R_h \mathrm{d}P\right) = \frac{1}{P}\left(\mathrm{d}A_0 - R_h \mathrm{d}P_0\right) + \mathrm{d}f(h)$ with $A_0 = W_0 h_0$ and $P_0 = W_0 + 2h_0$ respectively the unobserved low-flow area and perimeter under our modeling hypothesis (cf. section 2.2 and Fig. 1, see also Larnier et al. [1] for details on cross section representation). It follows that $f(h)$ is a function depending on the modeled water depth h and of the observed cross-section variation δA above low-flow (h_0), W_0 being defined from observables. We get $\mathrm{d}R_h = \frac{1}{P}\left(1 - \frac{2R_h}{W_0}\right)\mathrm{d}A_0 + \mathrm{d}f(h)$ and finally:

$$\mathrm{d}S_f = \frac{1}{K^2}\frac{Q}{A^2 R_h^{4/3}}\left(-2\frac{Q}{K}\mathrm{d}K - \frac{Q}{A}\left\{2 + \frac{4}{3}\left(1 - \frac{2R_h}{W_0}\right)\right\}\mathrm{d}A_0 + 2\mathrm{d}Q\right) - \mathrm{d}\phi(h) \tag{6}$$

with $\phi(h) = \frac{4}{3R_h^{7/3}}\frac{Q^2}{K^2 A^2}\mathrm{d}f(h)$ a function depending on the observed geometry of a cross section above low-flow and of the simulated flow (A, Q hence $h\,(A)$ given a channel geometry). We rewrite Eq. 6 as $\mathrm{d}S_f = \partial_K S_f \mathrm{d}K + \partial_{A_0} S_f \mathrm{d}A_0 + \partial_Q S_f \mathrm{d}Q - \mathrm{d}\phi(h)$ and under our modeling hypothesis we have $\partial_K S_f < 0$, $\partial_{A_0} S_f < 0$, $\partial_Q S_f > 0\ \forall x, t$, i.e. opposite effects of local values of friction K, low flow area A_0 and simulated local discharge Q values on S_f. Those terms are plotted on Fig. 10 along the Xingu River, on the model grid, from hydraulic variables simulated (forward run) with calibrated parameters (cf. Tab. 1). Note that $\mathrm{d}\phi(h)$ is not studied with this simple method.

Interestingly, $|\partial_K S_f|$ is about 100 times greater than $|\partial_{A_0} S_f|$ or $|\partial_Q S_f|$ at high-flow and about 10 times greater at low-flow. This is consistent with the singular value of friction that is found 1000 times greater than the one of reach averaged discharges by Garambois and Monnier [27] through a singular value decomposition of the normal equations of reach averaged Manning equations - applied to 70km of the Garonne River downstream of Toulouse (France). In other words, the friction term in the present 1D modeling context must be more sensitive to a change in friction than unknown low-flow bathymetry or discharge.

Remark that for low-flow, S_f is more sensitive to discharge than unknown cross sectional area ($|\partial_Q S_f| > |\partial_{A_0} S_f|$) and conversely for high-flow. Moreover the spatial variability of the three sensitivities is more pronouced at low-flow.

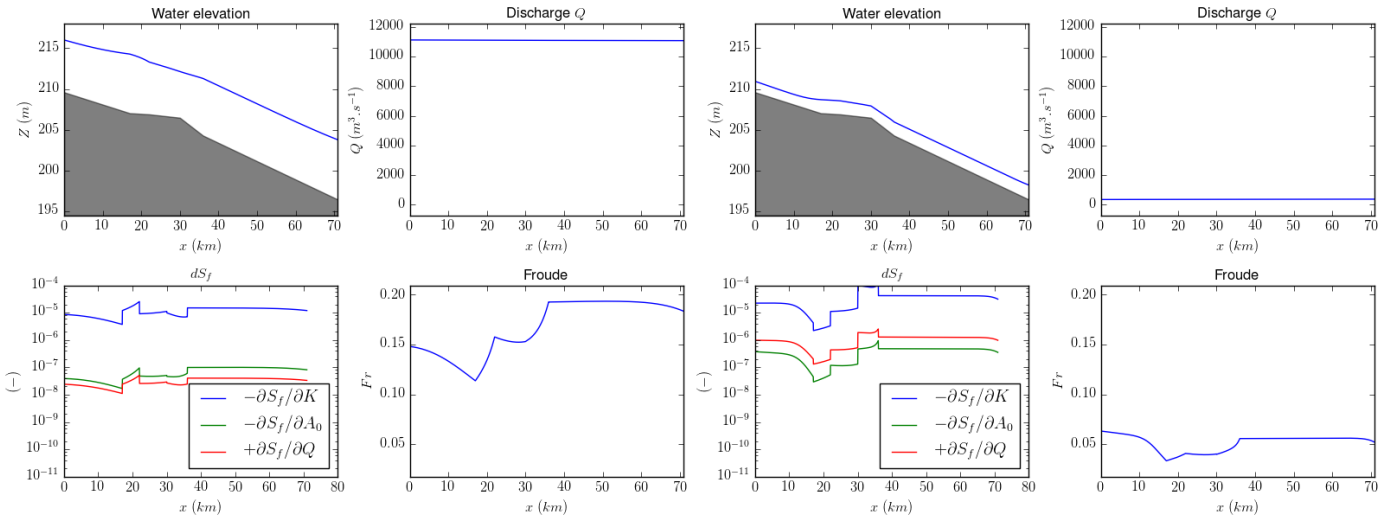

Figure 10: Evaluation of the partial derivatives of the friction source term S_f; forward run with the calibrated parameter set (cf. Tab. 1) and true inflow discharge.

Abrupt changes are highlighgted at locations corresponding to changes in the bottom slope or the channel width. The influences of the bottom slope break at $x = 30$km is clearly visible at low-flow and the influence of the width contraction at $x = 17$km at high-flow, which is fully consistent with the findings of [3]. Further investigations on the sensitivity of the full Saint-Venant equations, and especially the different contributions to the friction slope, in space and time could be of interest to better taylor, scale and constrain methods for tackling hydraulic inverse problems.

6. Conclusion

This paper investigates the challenging inference of the hydraulic triplet (discharge, bathymetry, friction) from real or synthetic altimetric WS observations only on an ungauged anabranching river.

The HiVDI inverse method presented in [1] is adapted for reproducing an anabranching flow by introducing *a spatially distributed* friction law depending on modeled water depth h and by using multi-satellite data.

The friction law coefficients are spatialized by reach to be coherent with the observation grid and with the (rather large) meaningful scale of these parameters in the 1D Manning-Strickler equation (see e.g. [61]). This effective modeling approach enables a fairly accurate reproduction of the anabranching flows observed during 8 years by nadir altimetry (ENVISAT) on this $71km$ anabranching river.

The inference capabilities of hydraulic parameters patterns from real altimetric observations along a single ENVISAT track or from the future spatially dense SWOT observations are demonstrated. For the present observed anabranching river complexity, the inverse method enables to infer a fairly realistic upstream discharge hydrograph along with an effective river channel. The estimated bathymetry and friction patterns somehow result in local

and effective stage-discharge relationships. In case of spatially sparse observations, the coherence between the sparse observation grid and the dense model grid is ensured using a piecewise linear bathymetry representation along with a friction power law with piecewise constant parameters. This constrain on the VDA process provided by the above defined effective bathymetry-friction representation by reach is highlighted with spatially sparse ENVISAT observations. Moreover the additional constrain provided by the forthcoming SWOT observations to infer a discharge hydrograph and densely distributed spatial controls is assessed on this effective anabranching river representation; the definition of friction by reaches enabling to consider more dense bathymetry controls.

SWOT observations would represent unprecedented measurements of hydrological and hydraulic processes signatures from the local to the hydrographic network scales, including complex flow zones such as anabranching ones. On-going researches focus on the detection and use of various hydraulic signatures in WS as highlighted here for bottom slope (resp. channel width) breaks in low (resp. high) flows (see WS curvature analysis and SW model behavior in [3]), on the estimation of reliable prior guesses on the sought parameters, model scaling and inverse problems at the scale of larger river network portions including complex flow zones.

Author contributions and acknowledgments

The contributions of the respective authors are as follows. Pierre-André Garambois designed the research plan and performed the numerical investigations and analysis. Pierre-André Garambois, Pascal Finaud-Guyot, Kevin Larnier and Amanda Montazem contributed to the hydraulic understanding and sensitivity analysis. Jérôme Monnier is the principal designer of the inverse computational method and its analysis. Jonas Verley has started the present study during the beginning of his PhD. This study is warmly dedicated to him.

The computational software DassFlow1D and satellite data curation toolbox were adapted from their previous versions ([1]) by Jonas Verley, Pierre-André Garambois and Kevin Larnier, this last generated the SWOT synthetic data using the large scale simulator and computational ressources of CNES ("Centre National d'Etudes Spatiales", French space agency); Amanda Montazem processed and analyzed the SWOT data. Stéphane Calmant provided the multisatelite dataset and interesting discussions related to the concept of *hydraulic visibility*.

The authors K. Larnier (software engineer at CS corp.) and J. Verley (software engineer during 10 months next PhD student IMT-INSA-CLS 17-18) have been co-funded by CNES. The four other authors have been partly supported by CNES TOSCA research project 14-18. The authors are indebted to Adrien Paris and Joecilla Da Silva for sharing data and for fruitfull discussions.

7. Appendix: the computational inverse method

As already briefly summarized in Section 2.3, the computational inverse method is based on Variational Data Assimilation (VDA) applied to the Saint-Venant flow model (1). The computational inverse method is those presented in [36, 1] with an augmented composite control vector c, see (4): c contains a spatially distributed friction

coefficient enabling to model complex flow zones (while it is an uniform friction law $K(h)$ in [1]). This definition of $K(x,h)$ enables to consider more heterogeneous bathymetry controls.

It is important to point out that the imposed downstream boundary condition is an unknown of the inverse problem. It is constrained with the observed water elevations and infered river bottom slope using a locally uniform flow hypothesis (i.e. Manning equation, cf. section 2.1).

The cost function $j(c)$ is defined as:

$$j(c) = j_{obs}(c) + \gamma\, j_{reg}(c) \tag{7}$$

where $\gamma > 0$ is a weighting coefficient of the so-called "regularization term" $j_{reg}(c)$. The term $j_{obs}(c)$ measures the misfit between observed and modeled WS elevations such that:

$$j_{obs}(c) = \frac{1}{2}\,\|(Z(\mathrm{c}) - Z_{obs})\|^2_{\mathcal{O}} \tag{8}$$

The norm $\|\cdot\|_{\mathcal{O}} = \|\mathcal{O}^{1/2}\cdot\|_2$ is defined from an a-priori positive definite covariance matrix $\mathcal{O}$. Assuming uncorrelated observations $\mathcal{O} = diag(\sigma_Z)$ with σ_Z the a-priori observation error on Z_{obs} - $\sigma_Z = 15cm$ in this study.

The modeled WS elevations Z depend on c through the hydrodynamic model (1) and the inverse problem reads as

$$c^* = \mathrm{argmin_c\ j}(c) \tag{9}$$

This optimal control problem is solved using a Quasi-Newton descent algorithm: the L-BFGS algorithm version presented in [62]. The cost gradient $\nabla j(c)$ is computed by solving the adjoint model; the latter is obtained by automatic differentiation using Tapenade software [63]. Detailed know-hows on VDA may be found e.g. in the online courses [64, 57].

To be solved efficiently this optimization problem needs to be "regularized". Indeed the friction and the bathymetry may trigger indiscernible surface signatures therefore leading to an ill-posed inverse problem; we refer e.g. to [59] for the theory of regularization of such inverse problems and to [1] for a discussion focused on the present inverse flow problem.

Following [1], the optimization problem (9) is regularized as follows. First the regularization term j_{reg} is added to the cost function, see (7). We simply set: $j_{reg}(c) = \frac{1}{2}\,\|b"(x)\|^2_2$. Therefore this term imposes (as weak constraint) the infered bathymetry profile $b(x)$ to be an elastic interpolating the values of b at the control points (i.e. a cubic spline).

A specificity of the present context is the inconsistency between the large observation grid (altimetry points) and the finer model grid. Between the sparse observations points (equivalently the control points), the bathymetry profile $b(x)$ is reconstructed as a piecewise linear function. It is worth to point out that the resulting reconstruction is consistent with the physical analysis presented in [20, 60, 3]. (This study analyses the adequation between the

SW model (1) behavior and the WS signature).

Next and following [65, 66, 1], the following change of control variable is made:

$$k = B^{-1/2}(\mathrm{c} - \mathrm{c}_{prior}) \tag{10}$$

where c is the original control vector, c_{prior} is a prior value of c and B is a covariance matrix. The choice of B is crucial in the VDA formulation; its expression is detailed below. After this change of variable the new optimization problem reads:

$$\min_k \mathrm{J}(k) \text{ with } \mathrm{J}(k) = j(c) \tag{11}$$

It is easy to show that this leads to the following new optimality condition: $B^{1/2}\nabla j(c) = 0$; somehow a preconditioned optimality condition. For more details and explanations we refer to [67, 68] and [1] in the present inversion context.

Assuming uncorrelated controls B is defined as a block-diagonal matrix:

$$B = \begin{pmatrix} B_Q & 0 & 0 & \\ 0 & B_b & 0 & \\ 0 & 0 & B_\alpha & \\ 0 & 0 & 0 & B_\beta \end{pmatrix} \tag{12}$$

Still following [1], the matrices B_Q and B_b are set as the classical second order auto-regressive correlation matrices :

$$(B_Q)_{i,j} = (\sigma_Q)^2 \exp\left(-\frac{|t_j - t_i|}{\Delta t_Q}\right) \text{ and } (B_b)_{i,j} = (\sigma_b)^2 \exp\left(-\frac{|x_j - x_i|}{L_b}\right) \tag{13}$$

The VDA parameters Δt_Q and L_b represent prior hydraulic scales and act as correlation lengths. Given the frequency (few days) and spatial resolution of observations (200m long "pixels" for SWOT), the low Froude anabranching river flows of interest, adequate values for those parameters are: $\Delta t_Q = 24$ h and $L_b = 3km$ km We refer to [36] for a thorough analysis of the discharge inference in terms of frequencies and wave lengths and Section 4.1 in the present river-observation context. In the present study, the friction parameters applied to deca-kilometric patches are assumed to be uncorrelated thus the matrices B_α and B_β are diagonal:

$$(B_\alpha)_{i,i} = (\sigma_\alpha)^2, (B_\beta)_{i,i} = (\sigma_\beta)^2 \tag{14}$$

The scalar values $\sigma_{\square}$ may be viewed as variances and constant values are used in this study: $\sigma_Q = 3500\,m^3/\mathrm{s}$, $\sigma_\alpha = 10\,m^{1/3}.s^{-1}$, $\sigma_\beta = 0.5$, $\sigma_b = 1\,m$.

8. References

[1] K. Larnier, J. Monnier, P.-A. Garambois, and J. Verley. River discharge and bathymetry estimations from swot altimetry measurements. -, -:–, 2019.

[2] Pierre-Andre Garambois, Stephane Calmant, Helene Roux, Adrien Paris, Jerome Monnier, Pascal Finaud-Guyot, Amanda Samine Montazem, and Joecila Santos-da Silva. Hydraulic visibility: Using satellite altimetry to parameterize a hydraulic model of an ungauged reach of a braided river. *Hydrological Processes*, 31(4): 756–767, 2017. ISSN 1099-1085. doi: 10.1002/hyp.11033. URL `http://dx.doi.org/10.1002/hyp.11033`. hyp.11033.

[3] A.-S. Montazem, P-A. Garambois, S. Calmant, P. Finaud-Guyot, J. Monnier, D. Medeiros Moreira, J. T. Minear, and S. Biancamaria. Wavelet-based river segmentation using hydraulic control-preserving water surface elevation profile properties. *Geophysical Research Letters*, 46(12):6534–6543, 2019. doi: 10.1029/2019GL082986. URL `https://agupubs.onlinelibrary.wiley.com/doi/abs/10.1029/2019GL082986`.

[4] World Meteorological Organization et al. The global observing system for climate: Implementation needs, 2016. URL `library.wmo.int/doc`$_n$$um.php?explnum_id = 3417$.

[5] B.M. Fekete and C.J. Vorosmarty. The current status of global river discharge monitoring and potential new technologies complementing traditional discharge measurements. *IAHS - PUB*, 2002.

[6] Charles J. Vorosmarty, Cort J. Willmott, Bhaskar J. Choudhury, Annette L. Schloss, Timothy K. Stearns, Scott M. Robeson, and Timothy J. Dorman. Analyzing the discharge regime of a large tropical river through remote sensing, ground-based climatic data, and modeling. *Water Resour. Res.*, 32:3137–3150, 1996. URL `http://dx.doi.org/10.1029/96WR01333`. 10.

[7] Douglas E. Alsdorf and Dennis P. Lettenmaier. Tracking fresh water from space. *Science*, 301(5639):1491–1494, 2003. doi: 10.1126/science.1089802. URL `http://www.sciencemag.org/content/301/5639/1491.short`.

[8] Stephane Calmant, Frederique Seyler, and Jean-Francois Cretaux. Monitoring continental surface waters by satellite altimetry. *Surveys in Geophysics*, 29(4-5):247–269, 2008. ISSN 0169-3298. doi: 10.1007/s10712-008-9051-1. URL `http://dx.doi.org/10.1007/s10712-008-9051-1`.

[9] G. J.-P. Schumann and A. Domeneghetti. Exploiting the proliferation of current and future satellite observations of rivers. *Hydrological Processes*, 30(16):2891–2896, 2016. doi: 10.1002/hyp.10825. URL https://onlinelibrary.wiley.com/doi/abs/10.1002/hyp.10825.

[10] Douglas E. Alsdorf, Ernesto RodrÃguez, and Dennis P. Lettenmaier. Measuring surface water from space. *Reviews of Geophysics*, 45(2), 2007. doi: 10.1029/2006RG000197. URL https://agupubs.onlinelibrary.wiley.com/doi/abs/10.1029/2006RG000197.

[11] M. Durand, L. Fu, D. P. Lettenmaier, D. E. Alsdorf, E. Rodriguez, and D. Esteban-Fernandez. The surface water and ocean topography mission: Observing terrestrial surface water and oceanic submesoscale eddies. *Proceedings of the IEEE*, 98(5):766–779, May 2010. doi: 10.1109/JPROC.2010.2043031.

[12] E. Rodriguez. SWOT Science requirements document. JPL document, JPL, 2012.

[13] Sylvain Biancamaria, Dennis P. Lettenmaier, and Tamlin M. Pavelsky. The swot mission and its capabilities for land hydrology. *Surveys in Geophysics*, 37(2):307–337, Mar 2016. ISSN 1573-0956. doi: 10.1007/s10712-015-9346-y. URL http://dx.doi.org/10.1007/s10712-015-9346-y.

[14] E. Rodriguez, Esteban-Fernandez D., E. Peral, C. W. Chen, J.-W. d. Blesser, and B. Williams. Wide-swath altimetry: A review. in d. stammer a. cazenave (eds.). *Satellite Altimetry over Oceans and Land Surfaces (Capter 2)*, page CRC press, 2018.

[15] Frederic Frappart, Stephane Calmant, Mathilde Cauhope, Frederique Seyler, and Anny Cazenave. Preliminary results of envisat ra-2-derived water levels validation over the amazon basin. *Remote Sensing of Environment*, 100(2):252 – 264, 2006. ISSN 0034-4257. doi: https://doi.org/10.1016/j.rse.2005.10.027. URL http://www.sciencedirect.com/science/article/pii/S0034425705003585.

[16] Charon M. Birkett. Contribution of the topex nasa radar altimeter to the global monitoring of large rivers and wetlands. *Water Resources Research*, 34(5):1223–1239, 1998. doi: 10.1029/98WR00124. URL https://agupubs.onlinelibrary.wiley.com/doi/abs/10.1029/98WR00124.

[17] Joecila Santos Da Silva, Frederique Seyler, Stephane Calmant, Otto Correa Rotunno Filho, Emmanuel Roux, Afonso Augusto Magalhaes Aranjo, and Jean Loup Guyot. Water level dynamics of amazon wetlands at the watershed scale by satellite altimetry. *International Journal of Remote Sensing*, 33(11):3323–3353, 2012. doi: 10.1080/01431161.2010.531914. URL http://dx.doi.org/10.1080/01431161.2010.531914.

[18] S. Calmant, J.-F. Cretaux, and F. Remy. 4 - principles of radar satellite altimetry for application on inland waters. In Nicolas Baghdadi and Mehrez Zribi, editors, *Microwave Remote Sensing of Land Surface*, pages 175 – 218. Elsevier, 2016. ISBN 978-1-78548-159-8. doi: https://doi.org/10.1016/B978-1-78548-159-8.50004-9. URL https://www.sciencedirect.com/science/article/pii/B9781785481598500049.

[19] George H. Allen and Tamlin M. Pavelsky. Global extent of rivers and streams. *Science*, 2018. ISSN 0036-8075. doi: 10.1126/science.aat0636. URL http://science.sciencemag.org/content/early/2018/06/27/science.aat0636.

[20] A. S. Montazem, P.-A. Garambois, S. Calmant, D. Medeiros Moreira, J. Monnier, and S. Biancamaria. Physical basis for river segmentation. In *AGU fall metting*, 2017.

[21] G. C. Nanson and A. D. Knighton. Anabranching rivers: Their cause, character and classification. *Earth Surface Processes and Landforms*, 21(3):217–239, 1996.

[22] Konstantinos M. Andreadis, Elizabeth A. Clark, Dennis P. Lettenmaier, and Douglas E. Alsdorf. Prospects for river discharge and depth estimation through assimilation of swath-altimetry into a raster-based hydrodynamics model. *Geophysical Research Letters*, 34(10), 2007. doi: 10.1029/2007GL029721. URL https://agupubs.onlinelibrary.wiley.com/doi/abs/10.1029/2007GL029721.

[23] S. Biancamaria, M. Durand, K.M. Andreadis, P.D. Bates, A. Boone, N.M. Mognard, E. Rodriguez, D.E. Alsdorf, D.P. Lettenmaier, and E.A. Clark. Assimilation of virtual wide swath altimetry to improve arctic river modeling. *Remote Sensing of Environment*, 115(2): 373 – 381, 2011. ISSN 0034-4257. doi: https://doi.org/10.1016/j.rse.2010.09.008. URL http://www.sciencedirect.com/science/article/pii/S0034425710002816.

[24] Michael Durand, Konstantinos M. Andreadis, Douglas E. Alsdorf, Dennis P. Lettenmaier, Delwyn Moller, and Matthew Wilson. Estimation of bathymetric depth and slope from data assimilation of swath altimetry into a hydrodynamic model. *Geophysical Research Letters*, 35(20), 2008. doi: 10.1029/2008GL034150. URL https://agupubs.onlinelibrary.wiley.com/doi/abs/10.1029/2008GL034150.

[25] Y. Yoon, M. Durand, C.J. Merry, E.A. Clark, K.M. Andreadis, and Alsdorf D.E. Estimating river bathymetry from data assimilation of synthetic swot measurements. *Journal of Hydrology*, 464 - 465 (0):363 – 375, 2012. ISSN 0022-1694. doi: http://dx.doi.org/10.1016/j.jhydrol.2012.07.028. URL http://www.sciencedirect.com/science/article/pii/S0022169412006294.

[26] Michael Durand, Jeffrey Neal, Ernesto Rodríguez, Konstantinos M Andreadis, Laurence C Smith, and Yeosang Yoon. Estimating reach-averaged discharge for the river severn from measurements of river water surface elevation and slope. *Journal of Hydrology*, 511:92–104, 2014.

[27] P-A. Garambois and J. Monnier. Inference of effective river properties from remotely sensed observations of water surface. *Advances in Water Resources*, 79:103–120, 2015.

[28] Colin J. Gleason and Laurence C. Smith. Toward global mapping of river discharge using satellite images and

at-many-stations hydraulic geometry. *Proceedings of the National Academy of Sciences*, 111(13):4788–4791, 2014. ISSN 0027-8424. doi: 10.1073/pnas.1317606111. URL http://www.pnas.org/content/111/13/4788.

[29] M. Durand, CJ. Gleason, P-A. Garambois, D. Bjerklie, LC. Smith, H. Roux, E. Rodriguez, PD. Bates, TM. Pavelsky, J Monnier, et al. An intercomparison of remote sensing river discharge estimation algorithms from measurements of river height, width, and slope. *Water Resources Research*, 2016.

[30] David M. Bjerklie, Charon M. Birkett, John W. Jones, Claudia Carabajal, Jennifer A. Rover, John W. Fulton, and Pierre-Andre Garambois. Satellite remote sensing estimation of river discharge: Application to the yukon river alaska. *Journal of Hydrology*, 561:1000 – 1018, 2018. ISSN 0022-1694. doi: https://doi.org/10.1016/j.jhydrol.2018.04.005. URL http://www.sciencedirect.com/science/article/pii/S0022169418302464.

[31] H. Roux and D. Dartus. Use of parameter optimization to estimate a flood wave: Potential applications to remote sensing of rivers. *J. of Hydrology*, 328:258–266, 2006.

[32] M. Honnorat, X. Lai, F-X. le Dimet, and J. Monnier. Variational data assimilation for 2D fluvial hydraulics simulation. *CMWR XVI-Computational Methods for Water Ressources. Copenhagen, june 2006.*, 2006.

[33] R. Hostache, X. Lai, J Monnier, and C. Puech. Assimilation of spatially distributed water levels into a shallow-water flood model. Part II: Use of a remote sensing image of Mosel River. *Journal of Hydrology*, 390:257–268, 2010. URL http://www.sciencedirect.com/science/article/pii/S0022169410004166. 3-4.

[34] X. Lai and J. Monnier. Assimilation of spatially distributed water levels into a shallow-water flood model. Part I: mathematical method and test case. *Journal of Hydrology*, 377:1–11, 2009. URL http://www.sciencedirect.com/science/article/pii/S0022169409004508. 1-2.

[35] DG Cacuci, IM , Navon, and M , Ionescu-Bugor. *Computational Methods for Data Evaluation and Assimilation*. Taylor and Francis CRC Press: Boca Raton, 2013.

[36] Pierre Brisset, Jérôme Monnier, Pierre-André Garambois, and Hélène Roux. On the assimilation of altimetric data in 1d saint–venant river flow models. *Advances in water resources*, 119:41–59, 2018.

[37] H. Oubanas, Igor Gejadze, Pierre-Olivier Malaterre, and F. Mercier. River discharge estimation from synthetic swot-type observations using var- iational data assimilation and the full saint-venant hydraulic model. *Journal of Hydrology*, pages Accepted, to appear, 2018.

[38] Igor Gejadze and Pierre-Olivier Malaterre. Discharge estimation under uncertainty using variational methods with application to the full saint-venant hydraulic network model. *International Journal for Numerical Methods in Fluids*, 83(5):405–430, 2017. ISSN 1097-0363. doi: 10.1002/fld.4273. URL http://dx.doi.org/10.1002/fld.4273. fld.4273.

[39] Y. Yoon, P-A. Garambois, R. Paiva, M. Durand, H. Roux, and E. Beighley. Improved error estimates of a discharge algorithm for remotely sensed river measurements: Test cases on Sacramento and Garonne Rivers. *Water Resources Research*, 52(1):278–294, 2016.

[40] S. Tuozzolo, G. Lind, B. Overstreet, J. Mangano, M. Fonstad, M. Hagemann, R. P. M. Frasson, K. Larnier, P.-A. Garambois, J. Monnier, and M. Durand. Estimating river discharge with swath altimetry: A proof of concept using airswot observations. *Geophysical Research Letters*, 0(ja), 2019. doi: 10.1029/2018GL080771. URL https://agupubs.onlinelibrary.wiley.com/doi/abs/10.1029/2018GL080771.

[41] A. F. Gessese, M. Sellier, E. Van Houten, and G. Smart. Reconstruction of river bed topography from free surface data using a direct numerical approach in one-dimensional shallow water flow. *Inverse Problems*, 27 (2):025001, 2011. URL http://stacks.iop.org/0266-5611/27/i=2/a=025001.

[42] R. Schneider, P. N. Godiksen, H. Villadsen, H. Madsen, and P. Bauer-Gottwein. Application of cryosat-2 altimetry data for river analysis and modelling. *Hydrology and Earth System Sciences*, 21(2):751–764, 2017. doi: 10.5194/hess-21-751-2017. URL https://www.hydrol-earth-syst-sci.net/21/751/2017/.

[43] Jochen E. Schubert, Wade W. Monsen, and Brett F. Sanders. Metric-resolution 2d river modeling at the macroscale: Computational methods and applications in a braided river. *Frontiers in Earth Science*, 3:74, 2015. ISSN 2296-6463. doi: 10.3389/feart.2015.00074. URL https://www.frontiersin.org/article/10.3389/feart.2015.00074.

[44] V.T. Chow. Handbook of applied hydrology. *McGraw-Hill Book Co., New-York, 1467 pages*, 1964.

[45] V. Guinot. *Wave Propagation in Fluids: Models and Numerical Techniques*, volume 16. 1993.

[46] David M. Bjerklie, S. Lawrence Dingman, and Carl H. Bolster. Comparison of constitutive flow resistance equations based on the manning and chezy equations applied to natural rivers. *Water Resources Research*, 41(11), 2005. doi: 10.1029/2004WR003776. URL https://agupubs.onlinelibrary.wiley.com/doi/abs/10.1029/2004WR003776.

[47] Rob Ferguson. Flow resistance equations for gravel- and boulder-bed streams. *Water Resources Research*, 43(5), 2007. doi: 10.1029/2006WR005422. URL https://agupubs.onlinelibrary.wiley.com/doi/abs/10.1029/2006WR005422.

[48] V.T. Chow. *Open-channel Hydraulics*. Mc Graw-Hill, New-York, USA, 1959.

[49] P-A. Garambois and J. Monnier. Inference of effective river properties from remotely sensed observations of water surface. *Advances in Water Resources*, 79:103–120, 2015.

[50] J. A. Cunge, M. Holly, F., and A. Verwey. *Practical Aspects of Computational River Hydraulics*. Pitam Publishing„ 1980.

[51] DassFlow. Data assimilation for free surface flows. Technical report, Mathematics Institute of Toulouse-INSA group-CS corp.-CNES-CNRS. http://www.math.univ-toulouse.fr/DassFlow, 2019. URL http://www.math.univ-toulouse.fr/DassFlow.

[52] A. Paris, R. Dias de Paiva, J. Santos da Silva, D. Medeiros Moreira, S. Calmant, P.-A. Garambois, W. Collischonn, M.-P. Bonnet, and F. Seyler. Stage-discharge rating curves based on satellite altimetry and modeled discharge in the amazon basin. *Water Resources Research*, 52(5):3787–3814, 2016. doi: 10.1002/2014WR016618. URL https://agupubs.onlinelibrary.wiley.com/doi/abs/10.1002/2014WR016618.

[53] Walter Collischonn, Daniel Allasia, B. Da Silva, and C. E. M. Tucci. The mgb-iph model for large-scale rainfallârunoff modelling. *Hydrological Sciences Journal*, 52(5):878–895, 2007. doi: 10.1623/hysj.52.5.878.

[54] R. Paiva, D. Costa Buarque, W. Collischonn, M.-P. Bonnet, F. Frappart, S. Calmant, and C. Bulhoes Mendes. Largeâscale hydrologic and hydrodynamic modeling of the amazon river basin. *Water Resources Research*, 49(3):1226–1243, 2013. doi: 10.1002/wrcr.20067. URL https://agupubs.onlinelibrary.wiley.com/doi/abs/10.1002/wrcr.20067.

[55] P. R. M. Pontes, F. M. Fan, A. S. Fleischmann, R. C. D. Paiva, D. C. Buarque, V. A. Siqueira, Pedro F. J., M. V. Sorribas, and W. Collischonn. Mgb-iph model for hydrological and hydraulic simulation of large floodplain river systems coupled with open source gis. *Environmental Modelling Software*, 94:1 – 20, 2017. ISSN 1364-8152. doi: https://doi.org/10.1016/j.envsoft.2017.03.029. URL http://www.sciencedirect.com/science/article/pii/S136481521630189X.

[56] J. Monnier, F. Couderc, D. Dartus, K. Larnier, R. Madec, and J-P. Vila. Inverse algorithms for 2D shallow water equations in presence of wet dry fronts. application to flood plain dynamics. *Advances in Water Resources*, 97:11–24, 2016.

[57] J. Monnier. *Variational data assimilation: from optimal control to large scale data assimilation*. Open Online Course, INSA Toulouse, 2014.

[58] Renato Prata de Moraes Frasson, Rui Wei, Michael Durand, J. Toby Minear, Alessio Domeneghetti, Guy Schumann, Brent A. Williams, Ernesto Rodriguez, Christophe Picamilh, Christine Lion, Tamlin Pavelsky, and Pierre-Andre Garambois. Automated river reach definition strategies: Applications for the surface water and ocean topography mission. *Water Resources Research*, 53(10):8164–8186, 2017. ISSN 1944-7973. doi: 10.1002/2017WR020887. URL http://dx.doi.org/10.1002/2017WR020887.

[59] Barbara Kaltenbacher, Andreas Neubauer, and Otmar Scherzer. *Iterative regularization methods for nonlinear ill-posed problems*, volume 6. Walter de Gruyter, 2008.

[60] Amanda Montazem. *Representation et segmentation hydraulique effective de rivieres pour le calcul de debit par altimetrie SWOT Ã l'echelle globale*. These de doctorat, Universite de Toulouse III Paul Sabatier, Toulouse, France, 2018.

[61] Vincent Guinot and Bernard Cappelaere. Sensitivity equations for the one-dimensional shallow water equations: Practical application to model calibration. *Journal of Hydrologic Engineering*, 14(8):858–861, 2009. doi: 10.1061/(ASCE)HE.1943-5584.0000061.

[62] J. C. Gilbert and C. Lemarechal. Some numerical experiments with variable-storage quasi-newton algorithms. *Mathematical programming*, 45(1-3):407–435, 1989.

[63] L. Hascoët and V. Pascual. The Tapenade Automatic Differentiation tool: Principles, Model, and Specification. *ACM Transactions On Mathematical Software*, 39(3), 2013. URL `http://dx.doi.org/10.1145/2450153.2450158`.

[64] F Bouttier and P Courtier. Data assimilation concepts and methods march 1999. *Meteorological training course lecture series. ECMWF*, page 59, 2002.

[65] A.C. Lorenc, S.P. Ballard, R.S. Bell, N.B. Ingleby, P.L.F. Andrews, D.M. Barker, J.R. Bray, A.M. Clayton, T. Dalby, D. Li, et al. The met. office global three-dimensional variational data assimilation scheme. *Quarterly Journal of the Royal Meteorological Society*, 126(570):2991–3012, 2000.

[66] A. Weaver and P. Courtier. Correlation modelling on the sphere using a generalized diffusion equation. *Quarterly Journal of the Royal Meteorological Society*, 127(575):1815–1846, 2001.

[67] Stephen A Haben, Amos S Lawless, and Nancy K Nichols. Conditioning and preconditioning of the variational data assimilation problem. *Computers & Fluids*, 46(1):252–256, 2011.

[68] Stephen A Haben, Amos S Lawless, and Nancy K Nichols. Conditioning of incremental variational data assimilation, with application to the met office system. *Tellus A*, 63(4):782–792, 2011.